Supporting Information

Directional Manipulation of Electron Transfer by Energy Level Engineering for Efficient Cathodic Oxygen Reduction

Yang Wang,[1a] Tianpei Zhou,[1 a] Shanshan Ruan,[1b] Hu Feng,[a] Wentuan Bi,[c] Jun Hu,[b] Ting Chen,[a] Hongfei Liu,[a] Bingkai Yuan,[a] Nan Zhang,[b] Wenjie Wang,[b] Lidong Zhang,[b] Wangsheng Chu,[b] Changzheng Wu*[a,c] and Yi Xie[a,c].

[a] School of Chemistry and Materials Science, Collaborative Innovation Center of Chemistry for Energy Materials, University of Science and Technology of China, Hefei, Anhui 230026, P. R. China.

[b] National Synchrotron Radiation Laboratory, University of Science and Technology of China, Hefei, Anhui 230026, P. R. China.

[c] Institute of Energy, Hefei Comprehensive National Science Center, Hefei, Anhui 230026, P. R. China.

[1]These authors contributed equally: Yang Wang, Tianpei Zhou and Shanshan Ruan.

* Correspondence: czwu@ustc.edu.cn

Experimental Details

Chemicals

4-nitrophthalonitrile, 3-nitrophthalonitrile and phthalonitrile were purchased from TCI in >99.0% purity. Anhydrous Iron(II) chloride ($FeCl_2$) was purchased from Alfa Aesar in 99.5% purity. Ammonium molybdate ($(NH_4)_2MoO_4$) was purchased from Macklin. Urea, Hydrochloric acid (HCl), Sodium hydroxide (NaOH), methanol (CH_3OH) and N, N-dimethylformamide (DMF) were purchased from Sino Pharm. Ketjenblak EC-600JD (KJ) was purchased from Japan Lion.

The synthesis of FePc-based molecular catalysts.

FePc-β-NO_2: 4-nitrophthalonitrile (10mmol, 1.73g) fragments was ground and evenly mixed with urea (80mmol, 4.80g) as nitrogen source, $FeCl_2$ (2.5mmol, 0.32g) as active iron source and trace amount of $(NH_4)_2MoO_4$ as solid-phase reaction catalyst, and then reacted at 200 ^oC under argon atmosphere for 8 hours. After cooling down to room temperature, the crude product was stirred in 1 M HCl solution for 1 h. The solid was filtered and then stirred in 1 M NaOH solution for 1 h. The crude product was filtered, washed with deionized water, dried in vacuum and then purified by Soxhlet extraction with methanol. After drying in vacuum, the targeted molecular precursor named FePc-β-NO_2 was obtained. High-resolution mass spectrometry gave a mass-to-charge (m/z) value of 747.0397.

FePc-α-NO_2: 3-nitrophthalonitrile (10mmol, 1.73g) fragments were ground and evenly mixed with urea (80mmol, 4.80g), $FeCl_2$ (2.5mmol, 0.32g) and trace amount of $(NH_4)_2MoO_4$, and then reacted at 200 ^oC under argon atmosphere for 8 hours. After cooling down to room temperature, the crude product was stirred in 1 M HCl solution for 1 h. The solid was filtered and then stirred in 1 M NaOH solution for 1 h. The crude product was filtered, washed with deionized water, dried in vacuum and then purified by Soxhlet extraction with methanol. After drying in vacuum, the targeted molecular precursor named FePc-α-NO_2 was obtained. High-resolution mass spectrometry gave a mass-to-charge (m/z) value of 747.0391.

FePc: Phthalonitrile (10mmol, 1.28g) fragments were ground and evenly mixed with urea (80mmol, 4.80g), $FeCl_2$ (2.5mmol, 0.32g) and trace amount of $(NH_4)_2MoO_4$, and then reacted at 200 ^oC under argon atmosphere for 8 hours. After cooling down to room temperature, the crude product was stirred in 1 M HCl solution for 1 h. The solid was filtered and then stirred in

1 M NaOH solution for 1 h. The crude product was filtered, washed with deionized water, dried in vacuum and then purified by Soxhlet extraction with methanol. After drying in vacuum, the targeted molecular precursor named FePc was obtained. High-resolution mass spectrometry gave a mass-to-charge (m/z) value of 567.0984.

The molecular catalysts were assembled by the π-π interaction between precursor molecules and porous Ketjen Black (KJ) carbon material. Generally, 30mg KJ dispersed into 30mL DMF with sonication for 0.5 hours. Then, a calculated amount of molecules was dissolved into 30mL DMF solvent. After, they were mixed together with using sonication for 0.5 hours, and stirred at room temperature for 24 hours. Subsequently, the mixture was centrifuged and the precipitate

was washed with DMF, ethanol and water. Finally, the precipitate was lyophilized to yield the final catalyst. Fe loadings of FePc-based molecular catalysts were all determined to be 2.1±0.16wt% by inductively coupled plasma-atomic emission spectrometer.

Characterizations. Synchrotron radiation photoelectron spectra (SRPES) experiments and soft X-ray absorption near-edge structure (XANES) were carried out at the Catalysis and Surface Science Endstation at the BL11U beamline in the National Synchrotron Radiation Laboratory (NSRL) in Hefei, China. High resolution mass spectrum (HRMS) was measured using Waters Acquity UPLC/XEVO G2-XS QTOF. Fourier Transform Infrared spectroscopy (FTIR) was recorded on a Thermo Nicolet FTIR spectrometer. Raman spectra was recorded on a LabRAM-HR Confocal Laser Micro Raman Spectrometer with excitation wavelength of 532 nm. Ultraviolet visible light spectrum (UV-VIS) was measured using a Shimadzu SolidSpec-3700. X-ray photoelectron spectrometer (XPS) measurements were carried out on an ESCALAB MK II X-ray photoelectron spectrometer with Mg-Ka as the excitation source. The loading content of Fe was measured on an inductively coupled plasma-atomic emission spectrometer (ICP-AES) by employing an Optima 7300 DV (PerkinElmer). High resolution transmission electron microscope (HRTEM) images, high-angle annular dark-field scanning transmission electron microscope (HAADF-STEM) images, and corresponding energy-dispersive spectroscopy (EDS) mapping profiles were tested on a JEOL JEM-ARF200F transmission/scanning transmission electron microscope with a spherical aberration corrector. Fe L-edge X-ray absorption spectra (XAS) were measured at the beamline U19 of national synchrotron radiation laboratory (NSRL, Hefei) in the total electron yield (TEY) mode by collecting the sample drain current under a vacuum better than 10^{-7} Pa. Fe K-edge XAS were carried out in fluorescence mode at the beamline 1W1B in Beijing Synchrotron Radiation Facility (BSRF, Beijing, China).

Electrochemical Measurements. The electrochemical tests were conducted with a three-electrode test mode on an electrochemical workstation (CHI660B). A glassy carbon (GC) electrode (diameter of 5 mm with surface area of 0.196 cm^2) was used as the working electrode, while a graphite rod and Ag/AgCl (3.5 M KCl) electrode were used as the counter electrode and reference electrode, respectively. All of the potentials were calibrated to the reversible hydrogen electrode (RHE) according to Nernst equation in 0.1 M KOH solution. In regards of preparing working electrode, 4 mg catalysts mixed with 40 μl Nafion solution (Sigma Aldrich, 5wt %) were dispersed in 1 ml of water-isopropanol solution with volume ratio of 3:1 by sonicating for at least 60 min to form a homogeneous ink. The catalyst ink was then drop-casted onto the glassy carbon electrode with a 0.6 mg cm^{-2} loading for all samples. Oxygen was used to purge the 0.1 M KOH solution for 30 min to keep the solution oxygen saturation before ORR testing. Before cyclic voltammetry (CV) and linear sweep voltammetry (LSV) tests, the working electrodes were activated by CV test at a scan rate of 50 mV s^{-1} for several times. The linear sweep voltammetry (LSV) was recorded at a scan rate of 10 mV s^{-1}. The kinetic current densities (J_K) were calculated according to Koutecky-Levich equation, at different electrode potentials:

$$\frac{1}{J} = \frac{1}{J_K} + \frac{1}{J_L} = \frac{1}{J_K} + \frac{1}{Bw^{1/2}} \qquad \text{equation 1}$$

$$B = 0.62nFC_0D_0^{2/3}v^{-1/6} \qquad \text{equation 2}$$

Where J is the measured current density, J_L is diffusion-limiting current density, w is the angular velocity, F is the Faraday constant (96485 C mol^{-1}), C_0 is the bulk concentration of O_2 (1.2×10^{-6} mol cm^{-3}), D_0 is the diffusion coefficient of O_2 in 0.1 M KOH (1.9×10^{-5} cm^2 s^{-1}) and v is the kinematic viscosity of the electrolyte (0.01 cm2 s^{-1}). Electrochemical impedance spectroscopy measurements were conducted in a frequency range from 0.01 Hz to 100000 Hz at 0.9 V vs RHE with an AC amplitude of 0.05V. The RRDE test was recorded at a scan rate of 10 mV s^{-1} and the ring electrode potential was set to 1.20 V versus RHE. The hydrogen peroxide yield (H_2O_2%) and electron transfer number (n) were calculated by the following equations:

$$H_2O_2 = 200 \times \frac{I_R}{I_D \times N + I_R} \qquad \text{equation 3}$$

$$n = 4 \times \frac{I_D \times N}{I_D \times N + I_R} \qquad \text{equation 4}$$

where I_R is the ring current, I_D is the disk current, and N = 0.4 is the current-collection efficiency of the platinum ring.

Zn-air battery tests. The homemade Zn-air fuel cell stack was schemed in Figure S15 and assembled according to the following steps: first of all, 6 mol/L KOH was used as electrolyte. Then, a polished zinc foil was used as the anode. Typically, the air electrode was fabricated by spraying catalyst ink onto the gas diffusion layer (purchased from Youteke Changzhou). The catalyst ink was prepared by mixing electrocatalysts with 5% Nafion solution and water/isopropanol solution (1:3 (v/v)). On average, 4 mg catalysts mixed with 40 μl Nafion solution (Sigma Aldrich, 5wt %) were dispersed in 1 ml of water/isopropanol solution. The electrocatalyst loading of air electrode is 2 mg cm^{-2} for this series catalysts. The test was conducted in air conditions without pumping oxygen.

DFT calculation method. All DFT calculations were performed by the Vienna ab initio simulation package (VASP), which delineates the electron core interactions based on the projector segmented wave (PAW) (1-4). The generalized gradient approximation (GGA) of Perdew-Burke-Ernzerhof (PBE) exchanged-correlation function was utilized to describe the electron-electron exchange (5). All systems were accounted for using spin polarization. The Brillouin zone was sampled using 1 × 1 × 1 gamma-centered Monkhorst-Pack k-point mesh (6).

A rectangular supercell containing 308 carbon atoms are used as substrate. A vacuum spacing of 30 Å is maintained normal to the surface to avoid spurious interactions in this direction. The dispersion-corrected DFT (DFT-D3) was employed to investigate the effect of van der Waals interactions on the adsorption of FePc-based molecules to the carbon substrate (7). Energy and force converge at 10^{-5} eV and 0.05 eV/Å, correspondingly. The cutoff energy was set of 450 eV. The calculations for the adsorption and desorption of O_2 and OH

intermediates by FePc-based molecular electrocatalysts were carried out by placing both adsorbate and substrate into 30 × 30 × 30 Å^3 box.

The adsorption energy is calculated according to the following equation:

$$E_{ads} = E^*_{sub} - (E_{sub} + E^*) \qquad \text{equation 5}$$

$$E_{des} = E_{sub} + E^* - E^*_{sub} \qquad \text{equation 6}$$

where E_{ads} is the adsorption energy, E_{des} is the desorption energy, E^*_{sub} is the total energy of the system of adsorbates adsorbed on substrates, E_{sub} and E^* are the energy of isolated substrates and isolated adsorbates, respectively. Adsorbates and substrates are represented with symbols of '*' and 'sub'.

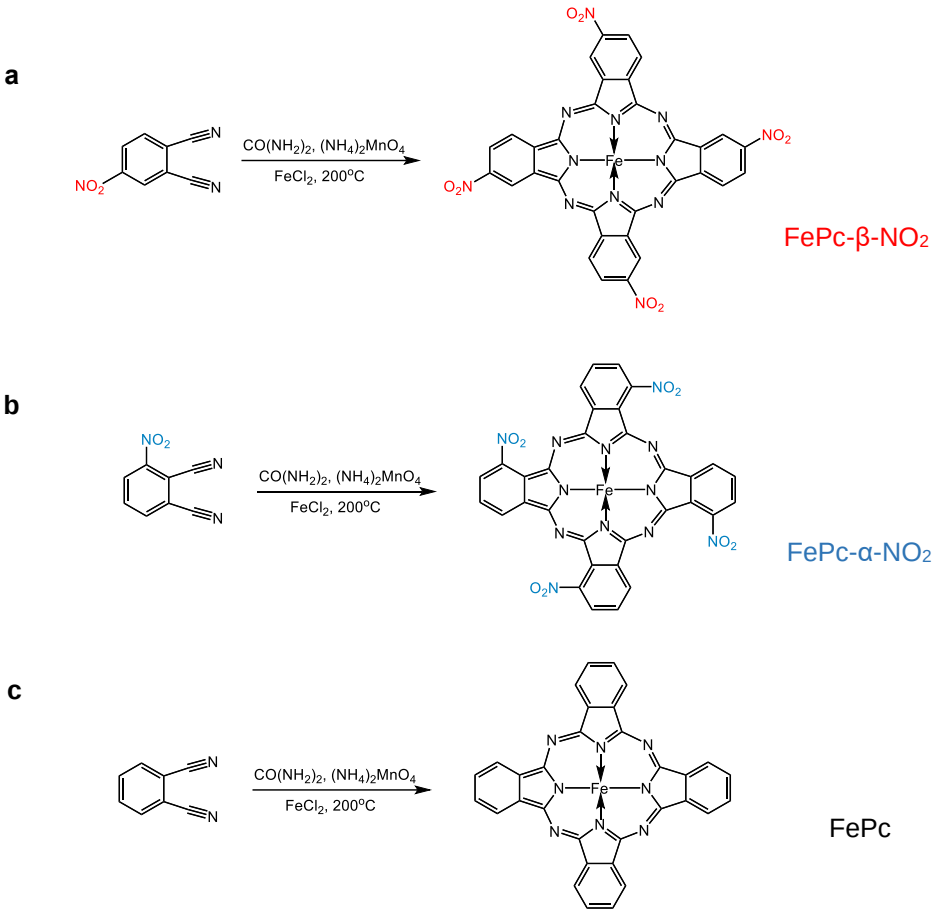

Figure S1. Schematic diagram of the molecular precursors synthesis routes for (a) FePc-β-NO_2, (b) FePc-α-NO_2 and (c) FePc.

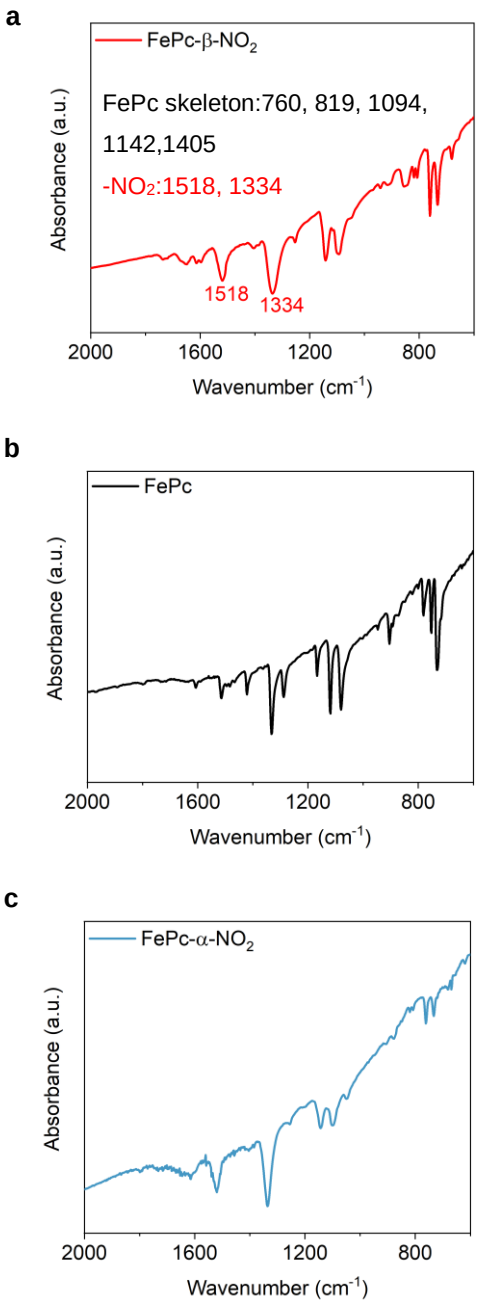

Figure S2. Fourier transform infrared spectra for (a) FePc-β-NO_2, (b) FePc and (c) FePc-α-NO_2.

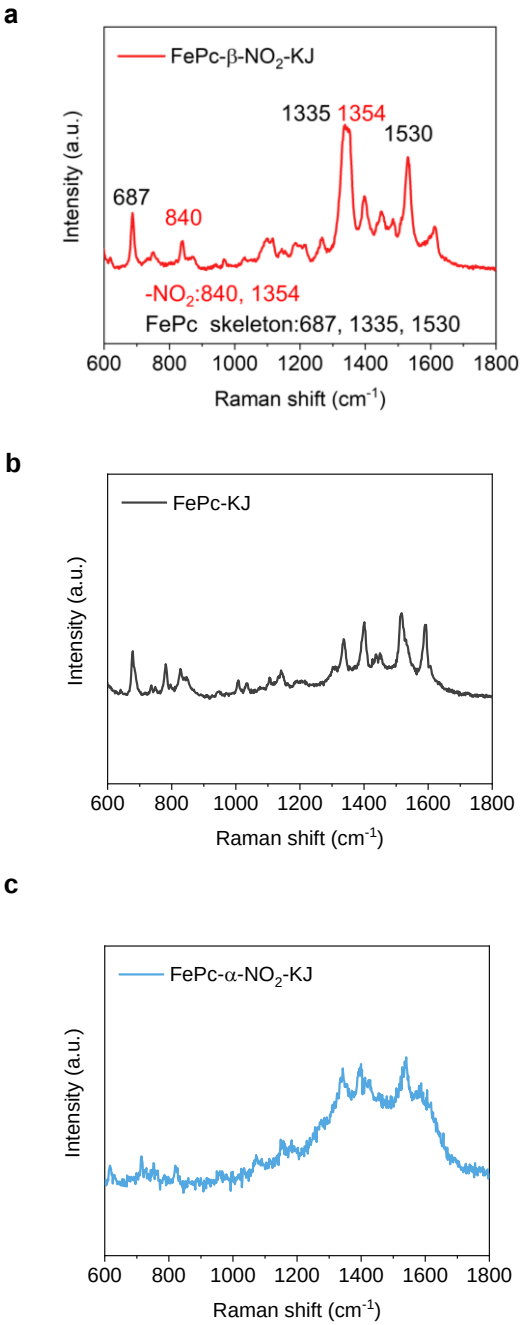

Figure S3. Raman spectra for (a) FePc-β-NO_2, (b) FePc and (c) FePc-α-NO_2.

Synchrotron radiation photoelectron spectra (SRPES) is employed to determine the energy level structure of FePc-based molecules and FePc-based molecule/carbon complexes with respect to the vacuum level (E_{VAC}=0 eV). The work function (W_F) was calculated by $W_F = h\nu - E_b$ from the secondary electron threshold, where the excitation photon energy (hv) is 40 eV. The binding energy (E_b) is converted by $E_b = h\nu - W_F(Instrument) - V_{bi} - E_k$, where the work function of instrument is 4.3 eV, the applied bias to the sample V_{bi} is -5 V, E_k is the kinetic energy measured directly by the instrument. Therefore, the calculated value of work function is 4.05, 4.26, 4.50 and 5.27 for FePc, Ketjen black carbon substrate, FePc-β-NO_2 and FePc-β-NO_2-KJ, respectively.

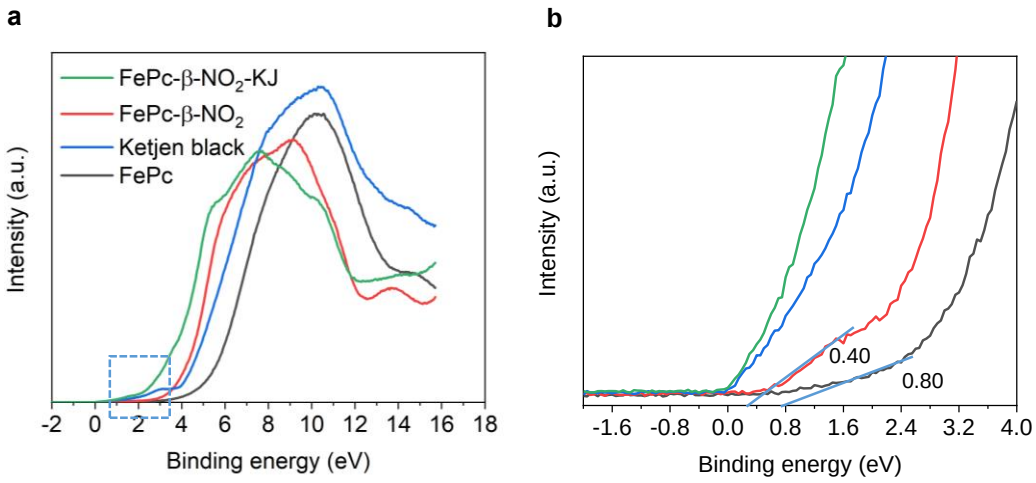

Figure S4. Synchrotron radiation photoelectron spectra (SRPES) of (a) valence band and (b) corresponding magnified region.

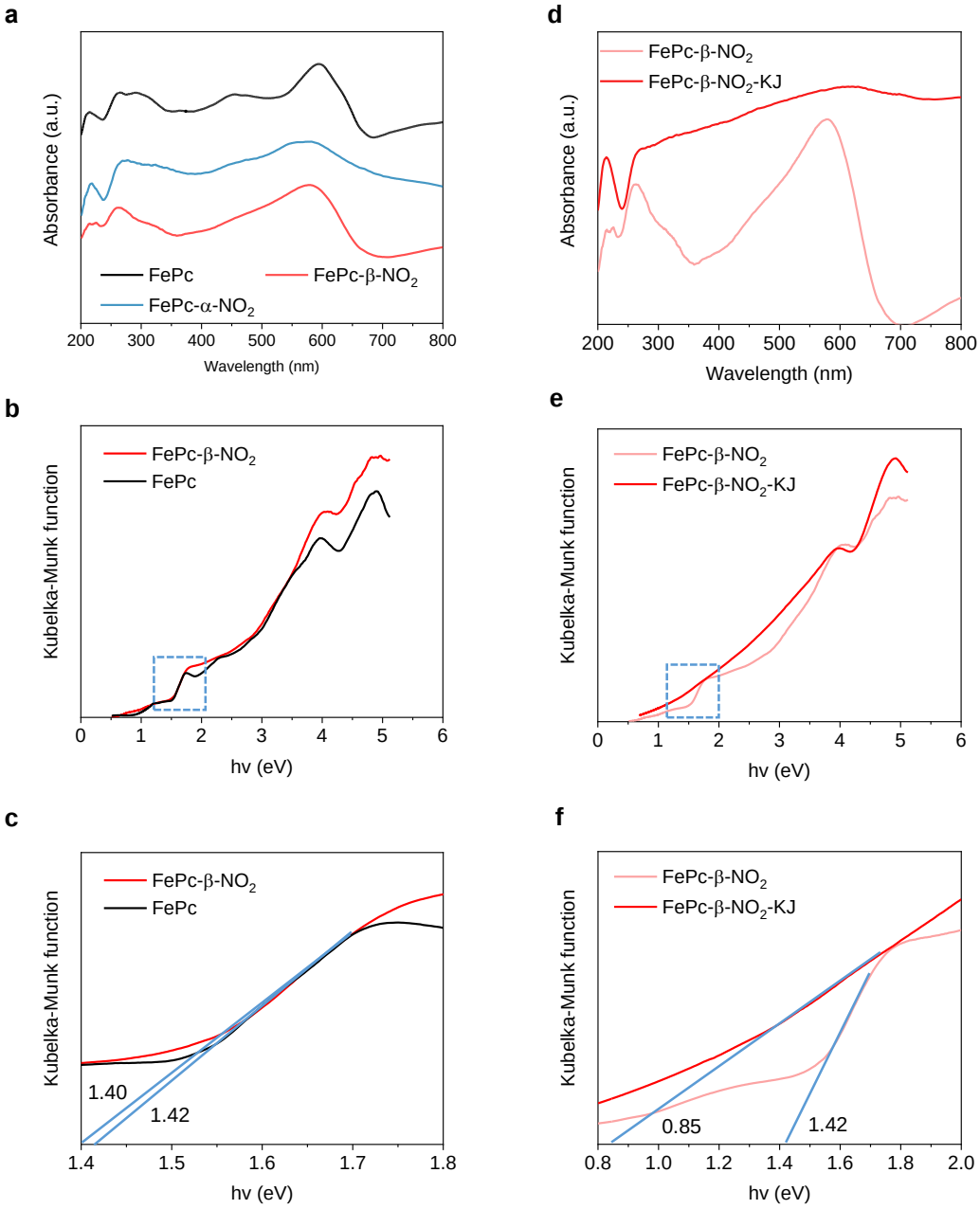

Figure S5. (a) UV-Vis spectrum of FePc-β-NO_2, FePc-α-NO_2 and FePc. The UV-Vis spectrum shows a typical peak distribution for FePc-based molecules composed of Q bands and B bands, as the results of π e^- transition from HOMO to LUMO, (b) Kubelka-Munk function of UV-VIS as function of hv, (c) corresponding magnified region. Eg (optical HOMO-LUMO energy level gap) is determined from c, which the value is 1.40 eV for FePc and 1.42 eV for FePc-β-NO_2. (d) UV-Vis spectrum of FePc-β-NO_2 and FePc-β- NO_2-KJ, (e) Kubelka-Munk function of UV-VIS as function of hv, (f) corresponding magnified region. After strong interaction with carbon, the transferred electrons were injected into LUMO of FePc-β-NO_2 molecule, inducing a depressed LUMO energy and narrow HOMO-LUMO gap from 1.42 to 0.85 eV.

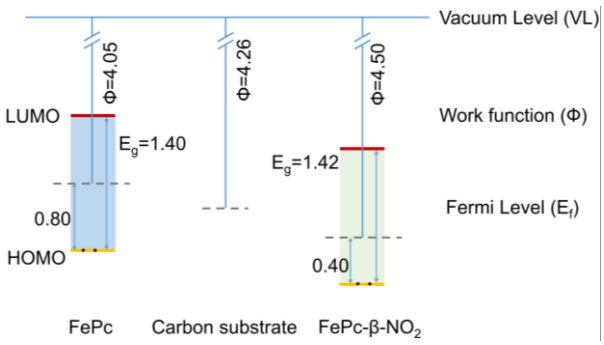

Figure S6. Detailed energy level information of FePc-β-NO_2, FePc and carbon.

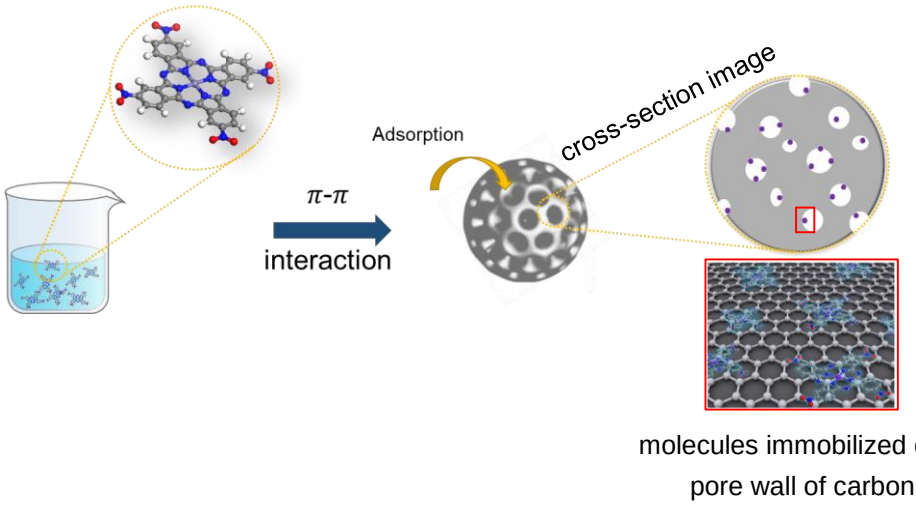

Figure S7. The scheme of catalysts assembly via π-π interaction between active molecules and porous carbon Ketjen Black (KJ).

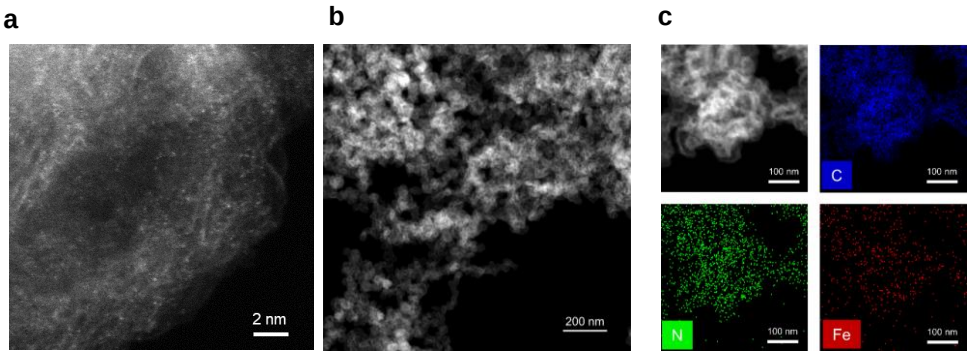

Figure S8. (a) HAADF-STEM, (b) TEM image and (c) EDS elemental mapping profiles for FePc-KJ molecular catalyst.

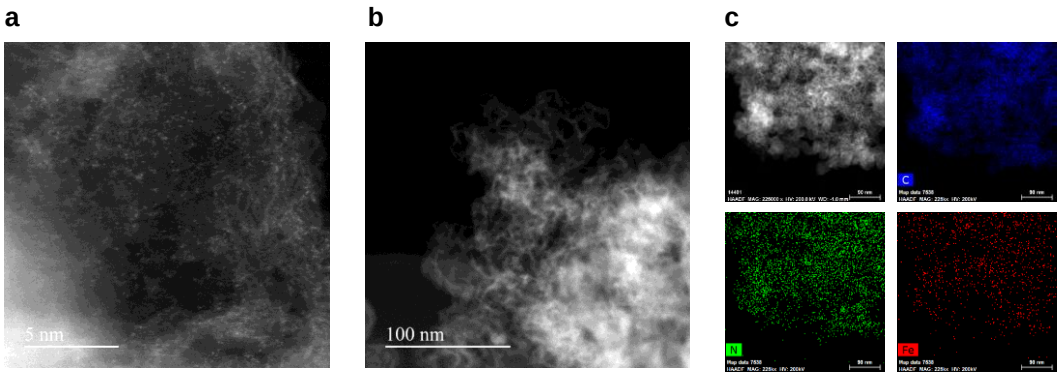

Figure S9. (a) HAADF-STEM, (b) TEM image and (c) EDS elemental mapping profiles for FePc-α-NO_2-KJ molecular catalyst.

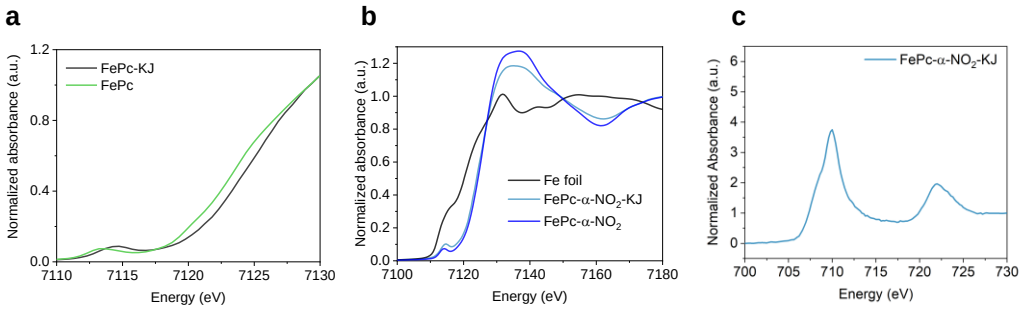

Figure S10. Fe K-edge XANES image for (a) FePc and FePc-KJ, (b) Fe foil, FePc-α-NO_2 and FePc-α-NO_2-KJ, (c) Fe L-edge X-ray absorption spectra of FePc-α-NO_2-KJ.

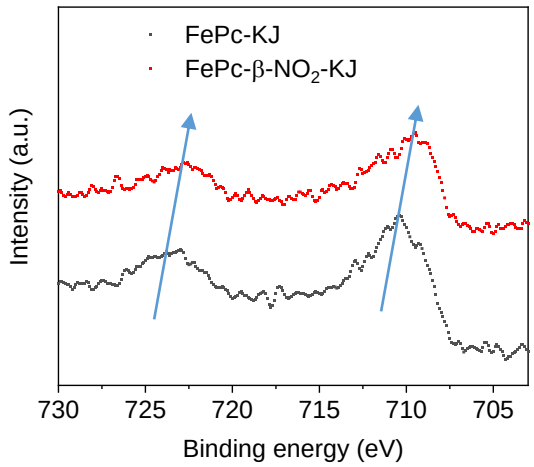

Figure S11. High-resolution Fe 2p XPS spectra for FePc and FePc-β-NO_2.

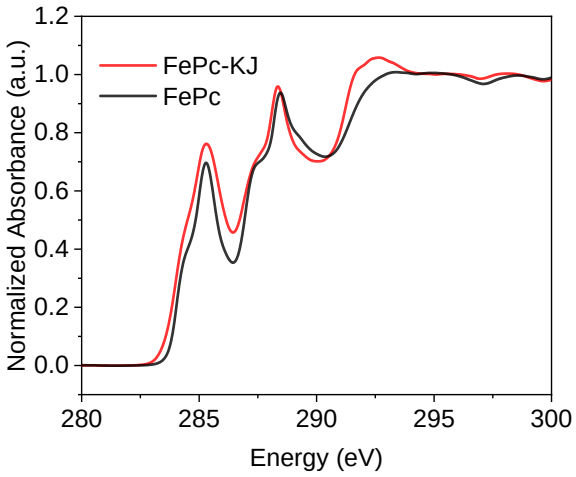

Figure S12. C K-edge soft X-ray absorption spectra of FePc molecule and FePc-KJ catalyst.

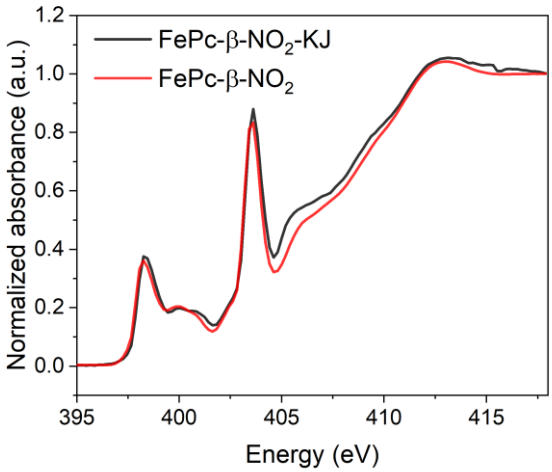

Figure S13. N K-edge soft X-ray absorption spectra of FePc-β-NO_2 and FePc-β-NO_2-KJ catalyst.

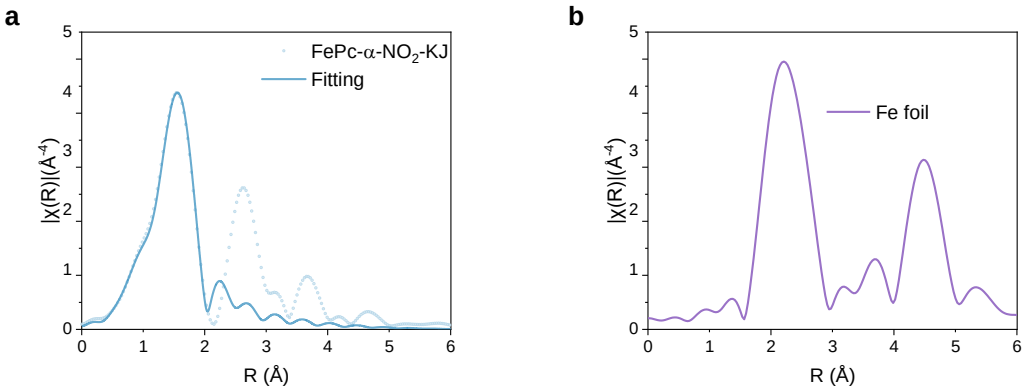

Figure S14. (a) R space fitting of FT-EXAFS spectra for FePc-α-NO_2-KJ, (b) R space of FT-EXAFS spectra for Fe foil.

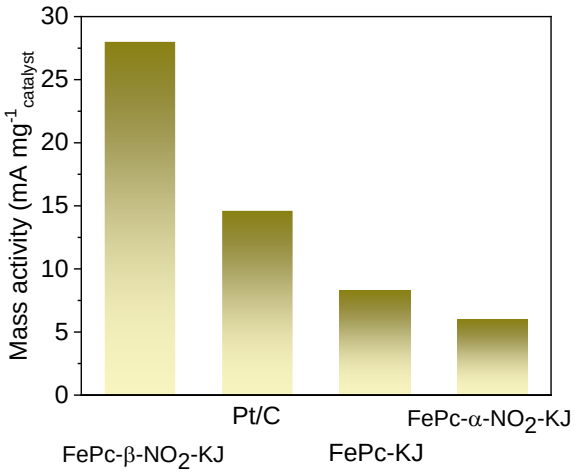

Figure S15. Mass activity at 0.90 V potential of FePc-β-NO_2-KJ, FePc-α-NO_2-KJ, FePc-KJ and Pt/C.

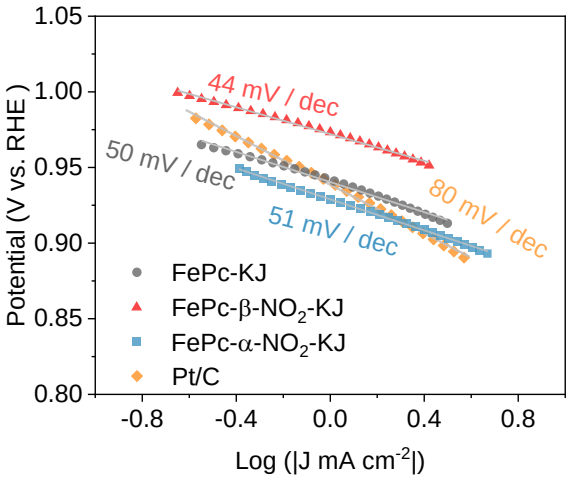

Figure S16. Tafel slope of FePc-β-NO_2-KJ, FePc-α-NO_2-KJ, FePc-KJ and Pt/C.

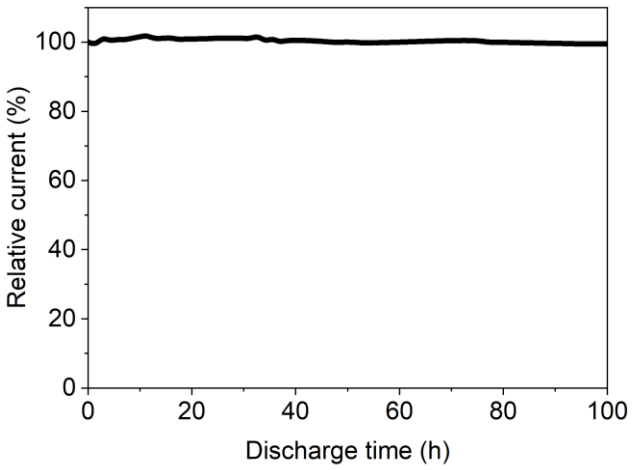

Figure S17. Long term discharge stability test at constant 0.8 V at saturated O_2 atmosphere with 800 rpm rotation rate for FePc-β-NO_2-KJ.

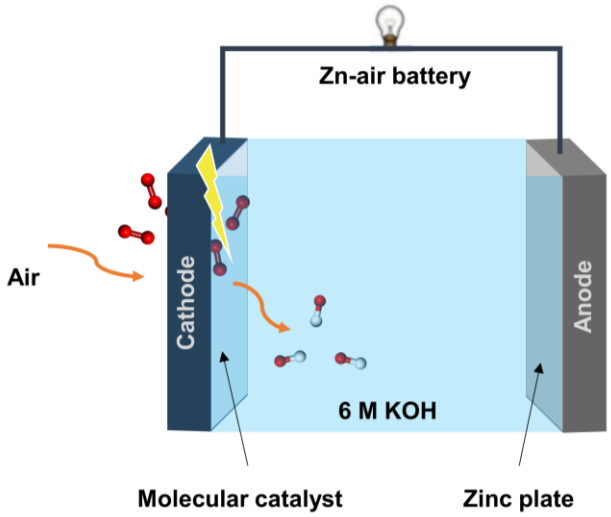

Figure S18. The configuration scheme of homemade Zn-Air battery stack.

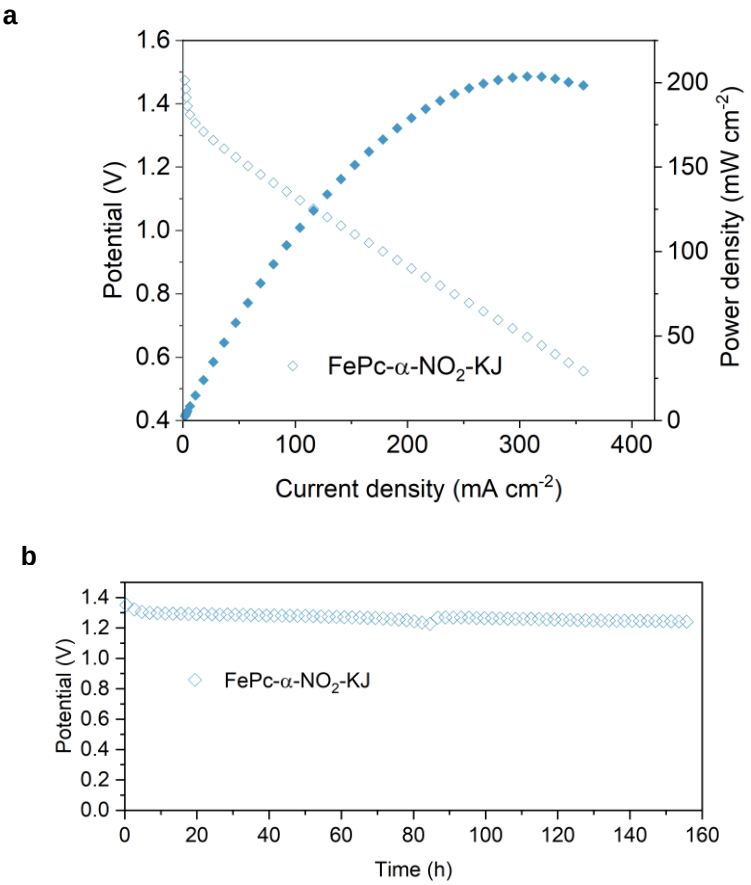

Figure S19. (a) Polarization and power density curves using FePc-α-NO_2-KJ as cathode catalysts in Zn-Air battery application, (b) The long-term discharge stability FePc-α-NO_2-KJ in Zn-Air battery.

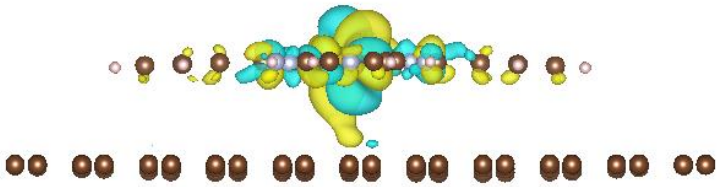

Figure S20. Differential charge density distribution of FePc-KJ.

Table S1. Fit results of Fe K-edge EXAFS for FePc-β-NO_2-KJ, FePc-α-NO_2-KJ and FePc-KJ.

Sample	Pair	N	R (Å)	$\Delta\sigma^2$ (10^{-3} Å^2)	E_0 (eV)	R factor
FePc-KJ	Fe-N/O	5.0 ± 0.2	2.05 ± 0.02	9.8 ± 0.4	4.09	0.014
FePc-β-NO_2-KJ	Fe-N/O	4.8 ± 0.2	1.98 ± 0.01	11.8 ± 0.4	4.09	0.003
FePc-α-NO_2-KJ	Fe-N/O	4.8 ± 0.2	2.02 ± 0.01	11.3 ± 0.2	4.09	0.001

Table S2. Summary of the ORR catalytic properties of reported Fe-N-C catalysts under alkali intermedia.

Catalyst	ORR performance (at 0.1 M KOH)		Zn-Air batteries performance		Ref
	$E_{1/2}$ (V vs. RHE)	stability	Peak power density	Battery stability	
FePc-β-NO_2-KJ	0.93 V (loading 0.6 mg cm^{-2})	20000 cycles or 100 hours I-t discharge	366 mW cm^{-2} (loading 2.0 mg cm^{-2})	160 hours at 5 mA cm^{-2}	This work
FeSAs/NSC	0.87 V (loading 0.2 mg cm^{-2})	5000 cycles	NA	NA	J. Am. Chem. Soc. 2019, 141, 51, 20118–20126
pf SAC-Fe-0.2	0.91 V (loading 0.255 mg cm^{-2})	6000 cycles	126.83 mW cm^{-2} (loading 0.5 mg cm^{-2})	5 hours at 100 mA cm^{-2}	Sci. Adv. 5, eaaw2322
FeAB–O	0.90 V (loading 0.2 mg cm^{-2})	2.8 hours I-t discharge	NA	NA	Nat. Commun. 2020, 11, 4173
Fe/N-G-SAC	0.89 V (loading 0.6 mg cm^{-2})	10000 cycles	120 mW cm^{-2} (loading 1.0 mg cm^{-2})	NA	Adv. Mater. 2020,32,2004900
FeN x@Fe/Fe3C	0.899 (loading 0.7 mg cm^{-2})	5000 cycles	NA	NA	J. Am. Chem. Soc. 2016, 138, 10, 3570-3578.
2D Fe−N−C	0.91 V (loading 0.4 mg cm^{-2})	12 mV decay after 6000 cycles	160 mW cm^{-2} (loading 0.5 mg cm^{-2})	135 hours at 5 mA cm^{-2}	ACS Materials. Lett. 2020, 2, 1, 35–41
CAN-Pc(Fe/Co)	0.84 V (loading 0.02 mg cm^{-2})	3.3 hours I-t discharge	88 mW cm^{-2} (loading 0.1 mg cm^{-2})	60 hours at 5 mA cm^{-2}	Angew. Chem. 2019, 131, 14866 - 14872
Fe-NCCs	0.82 V (loading 0.1 mg cm^{-2})	5000 cycles	70 mW cm^{-2} (loading 1.0 mg cm^{-2})	60 hours at 5 mA cm^{-2}	ACS Appl. Energy. Mater. 2018, 1, 9, 4982–4990
S,N-Fe/N/C-CNT	0.85 V (loading 0.6 mg cm^{-2})	10000 cycles	102.7 mW cm^{-2} (loading 1.25 mg cm^{-2})	NA	Angew. Chem. 2017, 129, 625 – 629
Fe–N-SCCFs	0.883 V (loading 0.24	10000 cycles	300 mW cm^{-2} (loading 1 mg	10 hours at 50 mA cm^{-2}	Nano lett. 2017, 17, 3: 2003-2009.

	mg cm^{-2})		cm^{-2})		
FeN_x-PNC	0.86 V (loading 0.14 mg cm^{-2})	20 mV decay after 10000 cycles	278 mW cm^{-2} (loading NA)	40 hours discharge-charge cycling at 5 mA cm^{-2}	ACS nano. 2018, 12(2): 1949-1958.
Fe-ISA/NC	0.896 V (loading 0.510 mg cm^{-2})	15000 cycles	NA	NA	Adv. Mater. 2018, 1800588
Fe-ISAs/CN	0.900 V (loading 0.408 mg cm^{-2})	5000 cycles	NA	NA	Angew. Chem. 2017, 56(24): 6937-6941.
Fe-N-HPe	0.910 V (loading 0.255 mg cm^{-2})	8 mV decay after 10000 cycles	164.8 mW cm^{-2} (loading 1.0 mg cm^{-2})	140 hours at 10 mA cm^{-2}	J. Mater. Chem. A. 2021, 9, 9761-9770
Fe50-N-C-900	0.92 V (loading 0.1 mg cm^{-2})	5.5 hours I-t discharge	NA	NA	Small. 2018, 14, 1703118
FeN_4-PN	0.91 V (loading 0.2 mg cm^{-2})	NA	NA	NA	ACS Catal. 2021, 11, 6304−6315
Fe–NC–SAC	0.90 V (loading 0.6 mg cm^{-2})	5000 cycles	NA	NA	Nat Commun. 2019, 1, 1278
Fe-NC-S	0.88 V (loading 0.2 mg cm^{-2})	NA	NA	NA	Chem.2020.10.027
FePc/CoPc HS	0.879 V (loading 0.05 mg cm^{-2})	35% decay after 2.8 hours I-t discharge	128 mW cm^{-2} (loading 1 mg cm^{-2})	NA	Adv. Funct. Mater. 2020, 2005000

References

(1) Kresse, G.; Hafner, J., Ab initio molecular dynamics for liquid metals. Physical review B 1993, 47, 558.

(2) Kresse, G.; Hafner, J., Ab initio molecular-dynamics simulation of the liquid-metal–amorphous-semiconductor transition in germanium. Physical Review B 1994, 49, 14251.

(3) Kresse, G.; Furthmüller, J., Efficient iterative schemes for ab initio total energy calculations using a plane-wave basis set. Physical review B 1996, 54, 11169.

(4) Kresse, G.; Joubert, D., From ultrasoft pseudopotentials to the projector augmented wave method. Physical review b 1999, 59, 1758.

(5) Perdew, J. P.; Burke, K.; Ernzerhof, M., Generalized gradient approximation made simple. Phys. Rev. Lett. 1996, 77, 3865.

(6) Monkhorst, H. J.; Pack, J. D., Special points for Brillouin zone integrations. Physical review B 1976, 13, 5188.

(7) Grimme, S.; Antony, J.; Ehrlich, S.; Krieg, H., A consistent and accurate ab initio parametrization of density functional dispersion correction (DFT-D) for the 94 elements H-Pu. J. Chem. Phys 2010, 132, 154104.